HANGING-CHAIN IMPACT DAMPERS: A SIMPLE METHOD FOR DAMPING TALL FLEXIBLE STRUCTURES

By Wilmer H. Reed III

NASA Langley Research Center
Langley Station, Hampton, Va., USA

Presented at the International Research Seminar:
Wind Effects on Buildings and Structures

Ottawa, Canada
September 11-15, 1967

HANGING-CHAIN IMPACT DAMPERS: A SIMPLE METHOD FOR DAMPING TALL FLEXIBLE STRUCTURES

By Wilmer H. Reed III
NASA Langley Research Center

ABSTRACT

This paper investigates a simple concept of achieving damping in order to suppress wind-induced oscillations of a class of erected structures such as antennas, stacks, and towers. It is shown that a chain, covered with a rubber sleeve and suspended with freedom to impact against a vertical channel, is capable of absorbing significant energy associated with transverse oscillations of the channel. The effects of various parameters on the performance characteristics of such a damper are determined experimentally in terms of mechanical impedance measurements. The experimental data are found to be in reasonable agreement with a simplified theory which is derived on the basis of a single-particle impact damper. Chain dampers installed on a 70-foot-tall erected launch vehicle increased the damping of the structure by a factor of up to 3. Results of this generalized research study indicate that the performance of hanging-chain impact dampers can be predicted with accuracy suitable for design purposes.

ACKNOWLEDGEMENTS

The author is indebted to Mr. William G. Johnson, Jr., who conducted the damper impedance tests, and to Messrs. Jerome T. Foughner and Rodney L. Duncan for their valuable assistance in performing the damper tests on the Jupiter launch vehicle.

HANGING-CHAIN IMPACT DAMPERS: A SIMPLE METHOD FOR DAMPING TALL FLEXIBLE STRUCTURES

By Wilmer H. Reed III*
NASA Langley Research Center

INTRODUCTION

Wind-excited oscillations of tall flexible structures can be significantly reduced by the addition of damping to the structure. This paper investigates a simple method of increasing the damping of such structures. The basic concept involves a chain that hangs in a vertical channel. A clearance gap is provided such that when the channel is attached to a vibrating structure the chain periodically impacts against the walls of the channel. Since these impacts provide the mechanism for dissipating vibration energy of the structure, the hanging-chain damper may be identified as belonging to a class of impact or acceleration dampers.

The first-known systematic research on impact dampers was conducted in 1940 by Arthur A. Regier at NACA/NASA Langley. Regier's study, which was unpublished, and a subsequent study by Lieber and Jensen (1945) treated the free vibration of a lightly damped structure to which is attached a mass particle in a container such that the particle is free to move relative to the container. These and more recent studies of impact dampers on idealized single-degree-of-freedom systems (Arnold (1957), Warburton (1957), Masri (1967), and Egle (1967)), have led to a reasonably good understanding of the phenomenon involved; however, at present few practical applications of impact dampers can be cited.

---

*Assistant Head, Aeroelasticity Branch, Dynamic Loads Division.

A recent practical problem, whose solution, incidentally, led to the present study of hanging-chain dampers, is reported by Farmer and Reed (1966), and Reed and Duncan (1967). This problem involved wind-excited oscillations of cylindrical masts utilized in U.S. Navy antenna systems. The antenna element is a 24-foot-tall cantilevered structure, the upper two-thirds of which is a 6-inch-diameter aluminum pipe. Oscillations of the mast in light to moderate winds are believed to be the cause of crack damage often observed in a load-carrying fiber-glass insulator at the base of the mast. A simple "fix" was found to be a small cluster of chains which were covered with plastic tubing and hung inside the tip of the mast. The effect of the chains, which weighed 12 pounds, was to increase the damping of the 260-pound antenna by a factor of about 20. Wind-tunnel tests of a full-scale antenna verified the effectiveness of the damper in bringing about significant reductions in vibration response.

The primary focus of this paper is on a generalized research investigation of chain impact dampers. By means of mechanical impedance measurements, the effects of various chain-damper parameters such as clearance gap, chain length and weight, amplitude and frequency of vibration are evaluated. These experimental data are then compared with predictions of a simplified theory.

Finally, an experiment involving the installation of chain dampers on a 70-foot-tall launch vehicle is described to illustrate the performance potentials of chain dampers on relatively large structures such as smokestacks and towers.

SYMBOLS

c_e equivalent viscous damping coefficient of damper

c_c critical damping, $2M\omega_n$

d	total clearance gap between chain and container
e	coefficient of restitution
$F(t)$	excitation force
F_o	fundamental component of $F(t)$
g	gravitational constant
i	$\sqrt{-1}$
k	structural spring constant
l	chain length
m	chain mass per unit length
m_p	mass of free particle in impact damper
m_e	effective mass of damper
M	lumped structural mass
N	number of impacts per cycle
$R(\omega), I(\omega)$	real and imaginary parts of fundamental components of $F(t)$
t	time
T	integration time used in impedance measurements
x	absolute displacement of damper mount
x_{st}	static deflection, F_o/k
y	absolute displacement of chain or free mass particle
Z_S, Z_D	mechanical impedance of structure and damper, respectively
δ	logarithmic decrement
μ	mass ratio, lm/M
φ	phase angle defining time of impact
ω	circular frequency
ω_1	fundamental frequency of hanging chain, $1.20\sqrt{g/l}$
ω_n	undamped natural frequency, $\sqrt{k/M}$

Subscripts:

-,+	conditions immediately before and immediately after impact
crit	critical gap ratio or frequency ratio above which steady-state impacts do not occur
opt	optimum damping
max	maximum

MECHANICAL IMPEDANCE OF IMPACT DAMPERS

Configurations Studied

The damper configuration chosen for study in this paper is shown schematically in figure 1. Parameters to be varied include the chain length l, the chain mass per unit length m, the gap distance d, and the amplitude and frequency of sinusoidal vibration. For all tests the chains were covered with a 1/16-inch-thick rubber sleeve which served to greatly reduce impact noises.

Basic Impedance Concepts

In previous investigations the performance of impact dampers has been evaluated usually in terms of the effect on response of a single-degree-of-freedom mass-spring system. Although the mass-spring system is one of fundamental importance, a somewhat more general approach based on mechanical impedance concepts will be followed in the present study. This alternate approach can be utilized to predict the effect of attaching a damper to an arbitrary structure whose impedance at the damper attachment point is known.

To illustrate impedance methods, figure 2 shows a chain damper mounted on a single-degree-of-freedom mass-spring oscillator. The force required to oscillate the damper container horizontally is expressed, for convenience, in terms

of an equivalent viscous damping coefficient c_e and an effective mass m_e. The total force required to drive the system with damper attached is then

$$F(t) = \left(M\ddot{x} + kx\right)_{structure} + \left(m_e\ddot{x} + c_e\dot{x}\right)_{damper} \tag{1}$$

For sinusoidal motions $x(t) = x_o e^{i\omega t}$ and $F(t) = F_o e^{i\omega t}$, equation (1) becomes

$$F_o = \left[Z_S(\omega) + Z_D(x,\omega)\right]\dot{x}_o \tag{2}$$

where

$$Z_S(\omega) = i\left(\omega M - \frac{k}{\omega}\right)$$

$$Z_D(x,\omega) = c_e + i\omega m_e$$

are the mechanical impedances of the structure and damper.* The damper impedance $Z_D(x,\omega)$ is expressed as a function of x as well as ω to indicate that, as will be shown later, the coefficients c_e and m_e depend on the amplitude of motion.

Equation (2) can be reduced to a convenient nondimensional form as follows:

$$\frac{x_{st}}{x_o} = \left[1 - \left(\frac{\omega}{\omega_n}\right)^2\left(1 + \mu\frac{m_e}{ml}\right)\right] + i\left[\mu\left(\frac{\omega}{\omega_n}\right)^2\frac{c_e}{ml\omega}\right] \tag{3}$$

---

*It should be noted that the force required to drive the damper in simple harmonic motion is not sinusoidal. It is instead a series of alternating impulses which occur twice per cycle when the chain impacts against the container wall. However, when $F(t)$ is expressed as a Fourier Series it can be shown that the energy dissipated per oscillation cycle is a function only of the fundamental component of the series. The term F_o in equation (2) is therefore taken to be the fundamental component of $F(t)$.

where

$$\mu = \frac{m\ell}{M}$$

$$x_{st} = \frac{F_o}{m\omega_n^2}$$

$$\omega_n^2 = \frac{k}{M}$$

The nondimensional damper parameters to be determined are $\frac{m_e}{m\ell}$ and $\frac{c_e}{m\ell\omega}$.

Test Apparatus and Data Reduction

Figure 3 shows a photograph and schematic diagram of the test apparatus with which damper parameters are measured. The damper is mounted on a light platform which is constrained, through flexures, to move horizontally. The platform is driven sinusoidally by a variable-speed electric motor connected by linkages to a high inertia flywheel. The driving force $F(t)$ is measured with a strain-gage load cell whose electrical output is amplified and fed to a sin-cos potentiometer. Since the potentiometer is mechanically connected to the flywheel drive shaft, its output voltages are proportional to $F(t)\cos \omega t$ and $F(t)\sin \omega t$. By use of analog computer components these products are integrated over a large number of cycles to obtain the fundamental components of $F(t)$ which are in phase and 90^o out of phase with the displacement. With $F(t)$ assumed to be of the form $m_e\ddot{x} + c_e\dot{x}$ and with $x = x_o \cos \omega t$ it can be shown that these integrations produce

$$R(\omega) = -\int_0^T F(t)\cos \omega t \, dt = -\frac{1}{2} m_e x_o \omega^2 T$$

$$I(\omega) = -\int_0^T F(t)\sin \omega t \, dt = -\frac{1}{2} c_e x_o \omega T$$

where the integration time T is large relative to the period of oscillation. (In these tests T was 20 seconds and the period varied from 2.0 to 0.2 sec.) Actually, the quantities m_e and c_e are determined from differences between the integrator outputs with and without the chain in the container. Thus, the container and oscillator platform masses are not included in m_e, and, similarly, the small residual damping in the platform support system is removed from c_e.

RESULTS AND DISCUSSION

Effect of Various Parameters on Chain Damper Impedance

Frequency.- A typical plot of damper parameters $\frac{c_e}{lm\omega}$ and $\frac{m_e}{lm}$ as a function of frequency is presented in figure 4. The frequency scale has been normalized with respect to fundamental natural frequency of a hanging chain, which is

$$\omega_1 = 1.20\sqrt{g/l}$$

Associated with these curves are three distinct regimes of chain vibration which were visually observed; these regimes are identified in figure 4 as I, II, and III. In region I, which extends from $\omega/\omega_1 = 1$ to approximately $\omega/\omega_1 = 3$, only a fraction of the chain length impacts against the container wall. Impact first occurs at the lower end of the chain when the forcing frequency coincides with fundamental chain frequency. With further increase in frequency, impact occurs over an increasingly greater portion of the chain until finally the chain impacts over virtually its entire length. Region II begins at this point and is characterized by a tendency for the impedance curves to level off at a constant value. Depending on the gap distance d (or more particularly the

nondimensional ratio d/x_o) the chain motion in Region II is found to follow one of two patterns: If the gap ratio is less than a critical value, the chain continues to impact along its full length for all higher frequencies and the impedance is essentially independent of frequency. This characteristic is shown in figure 4 by curves for $d/x_o = 1.72$. If the gap ratio is greater than about 4.0, however, there is a particular frequency at which chain vibration motions abruptly change. Below this critical frequency $\left(\omega/\omega_1\right)_{crit}$ the chain impacts twice per cycle against the container wall. For frequencies above the $\left(\omega/\omega_1\right)_{crit}$, Region III shown in figure 4 for $d/x_o = 4.78$, there are no impacts or irregular impacts and consequently the damping parameter abruptly drops to a low value. This low residual damping is believed to be associated with the friction forces in the vibrating chain. Also note that the in-phase impedance component m_e/ml changes sign at the critical frequency indicating that the reactance has changed from an inertia-type force to a spring-type force.

Further insight into this sudden change in system behavior with small frequency changes may be gained by examining the effects of another basic system parameter which is the gap-distance ratio d/x_o.

Gap distance.- Before experimental data are presented which show the effects of gap distance on damper impedance, it is helpful to first look at some theoretical predictions. As was previously noted in figure 4 when the driving frequency is greater than about 3 times the fundamental natural chain vibration frequency, impact occurs along the full chain length and damping is essentially independent of frequency. Thus, in Region II the chain damper appears to behave as a classical impact damper in which the damper mass is considered to be a single particle. In the Appendix of this paper theoretical expressions are derived for the impedance of a single-particle impact damper of the type

treated by previously mentioned investigators. In this analysis the chain is assumed to act as a vertical member which is free to translate laterally through a distance $\pm d/2$ relative to the container. Gravity restoring forces have been neglected and the particle mass is assumed to be $m\ell$, the total mass of the chain. With the assumption of two impacts per cycle the following equations are obtained in the Appendix

$$\frac{c_e}{\ell m\omega} = \frac{4}{\pi}\left(\frac{1 + e}{1 - e}\right)\sin^2\varphi \tag{4}$$

$$\frac{m_e}{\ell m} = \frac{4}{\pi}\left(\frac{1 + e}{1 - e}\right)\sin\varphi\cos\varphi \tag{5}$$

$$\frac{d}{x_o} = \left|\pi\left(\frac{1 + e}{1 - e}\right)\sin\varphi - 2\cos\varphi\right| \tag{6}$$

where e is the coefficient of restitution between the mass and container* and φ is a phase angle which specifies the container displacement at the time of impact.

The impedance parameters defined by these equations are plotted in figure 5 as a function d/x_o for specified values of e. An important fact to note in figure 5 is that for constant e the impedance parameters can be either of two possible values when $d/x_o \geqq 2.0$. From the experimental data shown in figure 6 it appears, however, that only the upper portion of the curves represents a stable solution. Furthermore, both theory and experiment indicate that, when d/x_o exceeds a certain critical value, impacts will no longer occur. Thus, associated with the critical frequency mentioned previously, there is similarly a critical gap ratio boundary separating a region of stable

*These equations apply when $e > 0$; when $e = 0$ alternate equations given by (A19) in Appendix apply.

steady-state impacts (Region II) from one of no impacts or intermittent impacts (Region III).

Restitution coefficient e.- The experimental curves shown in figure 6 are for different frequency ratios. These plots are to be compared with theoretical curves for which the e values were selected to best fit the experimental data. The values of e for the chains used in these experiments, although not accurately known, are believed to fall in the range shown in figure 6. Note in the figure that the lowest frequency ratio $\left(\omega/\omega_1 = 3.68\right)$ is associated with the highest coefficient of restitution (e = 0.40) and vice versa. Thus, it can be reasoned that if e does in fact fall off with increasing frequency in the manner shown in figure 6, then the critical frequency illustrated in figure 4 for the $d/x_o = 4.78$ curve can be interpreted as being the frequency associated with a particular e value for which $(d/x_o)_{crit} = 4.78$.

Although further study is required to explain more fully the mechanism which would cause e to vary with frequency, the following conjecture is offered. For a given gap distance, impact forces on the chain increase with increasing frequency. Static friction between adjoining chain links may be such that the chain acts essentially as a single body at low frequencies; at higher frequencies, where impact forces exceed the friction breakout forces, a portion of the energy formerly associated with rebound energy is now dissipated by friction between chain links, thus leading to a reduced e value.

Impact stability boundaries.- As indicated in the Appendix, regular two-impact-per-cycle motion of the system is possible only for a particular range of e and d/x_o values. Beyond the boundaries of this range, impacts either do not occur or there are more than two impacts per cycle. These boundaries are presented in figure 7. The curve on the right defines the upper limit

of d/x_o for which there are two impacts per cycle. The $(d/x_o)_{crit}$ value discussed in the previous figure would correspond to points on this boundary. The curve on the left defines the lower limit of d/x_o for two-impact-per-cycle motions. This boundary also appears in figure 5 as the line which terminates the family of curves as d/x_o approaches zero. For d/x_o values below this lower limit the rebound velocity of the mass relative to the container is such that after an initial impact against one side of the container the container overtakes the mass causing a second impact. Although in this region where $N > 2$ the assumptions of the analysis no longer hold, the damper does not necessarily become ineffective as it does when the right-hand boundary is crossed in going from regions $N = 2$ to $N = 0$.

To further define impact stability boundaries, data obtained on all chain-damper configurations of this study are summarized in figure 8. This figure shows the experimentally determined relationship between the parameters $(d/x_o)_{crit}$ and $\left(\omega/\omega_1\right)_{crit}$ which were discussed previously in figures 4 and 6. Also indicated by a second ordinate in figure 8 are the e values associated with the theoretical stability boundary between $N = 2$ and $N = 0$ in figure 7. Note that with increasing frequency the experimental stability boundary appears to asymptotically approach the minimum value predicted by theory which is $(d/x_o)_{crit} = 3.75$ with $e = 0$. (See fig. 7 and Appendix.)

Optimum Damper Performance

From the family of damping curves plotted in figure 5, it is evident that for a given d/x_o there is a particular e for which damping is maximum, and similarly for a given e there is an optimum value of d/x_o. As indicated by equation (4) maximum damping occurs when $\varphi = \pi/2$. The impedance parameters for

optimum damping are therefore

$$\left.\begin{aligned}\left(\frac{c_e}{lm\omega}\right)_{opt} &= \frac{4}{\pi}\left(\frac{1+e}{1-e}\right)\\ \left(\frac{m_e}{lm}\right)_{opt} &= 0\end{aligned}\right\} \tag{7}$$

The corresponding optimum gap ratio is from equation (6)

$$\left(\frac{d}{x_o}\right)_{opt} = \pi\left(\frac{1+e}{1-e}\right) \tag{8}$$

Thus, when equations (7) and (8) are combined the following equation for the loci of maximum damping as a function of gap distance is obtained

$$\left(\frac{c_e}{lm\omega}\right)_{opt} = \frac{4}{\pi^2}\left(\frac{d}{x_o}\right)_{opt} \tag{9}$$

An interesting feature of this equation is that it does not depend explicitly upon the coefficient of restitution e. Since e is essentially an undetermined parameter in the present study of chain dampers, equation (9) suggests another summary-type presentation of the experimental data. Accordingly, a compilation of all $\left(c_e/lm\omega\right)_{opt}$ values obtained during the tests are plotted in figure 9 against the corresponding value of (d/x_o).

The data points in figure 9 encompass not only variations in the length and running mass of the chain, as indicated by the symbols, but also independent variations of d and x_o. In addition, the points cover frequency ratio variations from approximately $\omega/\omega_1 = 2.0$ to $\omega/\omega_1 = 7.0$. As noted previously, the lower frequencies are associated with the higher damping values and vice versa.

It may be concluded from experimental data presented in this and preceding figures that the performance of chain dampers can be predicted with reasonable

accuracy by theory for a single mass impact damper providing an account is taken of the inferred variation of e with frequency ratio.

APPLICATION OF RESULTS FOR SINGLE-DEGREE-OF-FREEDOM SYSTEM

Having evaluated the mechanical impedance characteristics of chain dampers let us next attempt to interpret these results in terms of forced response of a single-degree-of-freedom mass-spring oscillator with a chain damper attached. The particular quantity of interest will be the amplitude of maximum response.

With reference to equation (3) it will be assumed that the forced response amplitude ratio x_o/x_{st} is maximum $\left(x_{st}/x_o = \text{minimum}\right)$ at a frequency which causes the real part of equation (3) to vanish. This frequency is

$$\frac{\omega}{\omega_n} = \frac{1}{\sqrt{1 + \mu \frac{m_e}{ml}}} \tag{10}$$

which when substituted into the imaginary part of equation (3) gives for the amplitude of maximum response

$$\left|\frac{x_o}{x_{st}}\right|_{max} = \frac{1 + \mu \frac{m_e}{ml}}{\mu \frac{c_e}{lm\omega}} \tag{11}$$

If the damper operates under optimum conditions as given by equation (7) the maximum response equation becomes

$$\left|\frac{x_o}{x_{st}}\right|_{max} = \frac{\pi(1 - e)}{4\mu(1 + e)} \tag{12}$$

and the associated optimum gap distance in terms of static deflection is from equations (8) and (12)

$$\left(\frac{d}{x_{st}}\right)_{opt} = \left(\frac{d}{x_o}\right)_{opt}\left(\frac{x_o}{x_{st}}\right)_{max}$$

$$= \frac{\pi^2}{4\mu} \tag{13}$$

Equivalent expressions derived by Arnold (1957) and Warburton (1957) for $\omega/\omega_n = 1$ are

$$\left|\frac{x_o}{x_{st}}\right|_{max} = \frac{\pi(1 + \mu)(1 - e)}{4\mu(1 + e)} \tag{14}$$

and

$$\left(\frac{d}{x_{st}}\right)_{opt} = \frac{\pi^2}{4\mu} + 1 \tag{15}$$

On the basis of experimentally determined chain damper impedance data it appears that for a conservative estimate of optimum damper performance one could assume $\frac{c_e}{l_m\omega} = 2.0$ and $\frac{m_e}{l_m} = 1.0$. These values with equations (9) and (11) lead to the following expressions for maximum response and the maximum gap distance

$$\left|\frac{x_o}{x_{st}}\right|_{max} = \frac{1 + \mu}{2\mu} \tag{16}$$

and

$$\left(\frac{d}{x_{st}}\right)_{opt} = \frac{\pi^2}{4\mu}(1 + \mu) \tag{17}$$

It is interesting to note that if a value of $e = 0.22$ is used in equation (14), equation (16) is obtained.

It is also informative to compare the optimum performance of chain dampers with that of equivalent linear viscous damping. The maximum response of a

lightly damped structure with viscous damping is

$$\left|\frac{x}{x_{st}}\right|_{max} = \frac{1}{2\,\frac{c}{c_c}} \tag{18}$$

Thus, by equating equations (16) and (18) it is found that a chain damper under best operating conditions is equivalent to a viscous damping ratio of

$$\left(\frac{c}{c_c}\right)_{equiv} = \frac{\mu}{1+\mu} \tag{19}$$

CHAIN DAMPER INSTALLATION ON AN ERECTED LAUNCH VEHICLE

In order to evaluate the performance of chain dampers on an actual structure, an experimental damper installation was attached to a 70-foot-tall Jupiter vehicle at Wallops Island, Virginia. This surplus vehicle had been used previously by Foughner and Duncan (1966) in an extensive research program to study the effects of ground wind loads on erected launch vehicles, and was therefore fully instrumented for dynamic response measurements.

The damper installation on the vehicle is shown in figure 10. A 4-foot-wide band of 1/32-inch sheet metal, bent to form a series of vertical channels, was wrapped around the vehicle near the top. With the vehicle skin as an inner wall, fifty six 2- by 4-inch channels were formed. Half of these channels were divided by sheet-metal inserts which split the 2- by 4-inch channel into two 2- by 2-inch channels giving a total of 84 channels. A 40-inch-long, 6-pound chain covered with a rubber sleeve was hung in each channel. These chains were the heaviest of the three chain configurations evaluated in the impedance tests (3/8-inch link size, 0.148 lb per ft). The total damper-chain weight was about 500 pounds which is approximately 5 percent of the vehicle weight without dampers. The fundamental natural cantilever bending

frequency of the vehicle alone is 2.0 Hz which is about 3 times greater than the fundamental chain frequency $\omega_n/\omega_1 \approx 3.0$. Also, the clearance gaps between the chain and the channel walls is 0.45 inch and 2.45 inches for the 2-inch and 4-inch channel sides, respectively.

The effect of chain dampers on free vibration response of the vehicle in its fundamental mode is as shown in figure 11. This figure presents the logarithmic decrement of successive vibration cycles as a function of the vehicle displacement amplitude at the center of the damper. The vibration time histories from which the decrements were obtained are also presented in the figure.

Note that the damper has maximum effectiveness for amplitudes between 0.075 and 0.15. For vibrations in the direction of the narrow channel dimension these amplitudes are equivalent to d/x_o ratios of 6.0 and 3.2 which, as previously indicated, falls within the damper stability boundary for 2-inpact-per-cycle motion (see fig. 8 at $\omega/\omega_1 = 3.0$). For motion parallel to the 4-inch channel dimension, however, the chains in the rectangular channel are ineffective since d/x_o is always greater than 10.0. (The highest critical d/x_o ratio obtained in the impedance test was 8.) Also, it is evident that at very low amplitudes the damper effectiveness is lost because the d/x_o ratio for all chains has exceeded the critical value for which impacts are possible. To extend effective damper operation over a broader range of amplitudes, one might use more variations in the gap distance or, as suggested by Reed and Duncan (1967), tapered channels.

CONCLUDING REMARKS

This paper investigates a simple concept of achieving damping in a class of erected structures such as antennas, stacks, and towers. It is shown that a

chain, covered with a rubber sleeve and suspended with freedom to impact against a vertical channel, is capable of absorbing significant energy associated with transverse oscillations of the channel. The performance characteristics of such a damper are determined experimentally in terms of mechanical impedance measurements. Experimental data are presented to show the effects of such parameters as length and mass of the chain, clearance gap distance, and amplitude and frequency of forced sinusoidal motion. These data are found to be in reasonable agreement with a simplified theory which is derived in the Appendix of the paper on the basis of a single-particle impact damper.

In an experiment to evaluate performance of this type damper on a relatively large structure, chain dampers were installed on a 70-foot-tall erected launch vehicle. It is shown that the damper, which weighed about 5 percent of the vehicle weight, increased the damping of the structure by a factor of up to 3.

From results of this generalized research study it is felt that the performance of hanging-chain impact dampers can be predicted with accuracy suitable for design purposes.

APPENDIX

IMPACT DAMPER ANALYSIS

Derivation of Impedance Equations

The idealized impact damper to be considered is shown in figure 12. A frictionless mass particle m_p is free to oscillate in a container within a clearance gap distance d. Let $F(t)$ be the force required to drive the container sinusoidally at a prescribed amplitude x_o and frequency ω, and let $y(t)$ be the absolute displacement of m_p. It is assumed that twice per cycle, at equally spaced time intervals π/ω, the particle impacts against either end of the container. The time of impact is defined by the phase angle φ in the container displacement equation

$$x(t) = x_o \cos(\omega t + \varphi) \tag{A1}$$

such that impacts occur when the displacement is $x_o \cos \varphi$, $x_o \cos(\varphi + \pi)$, etc.

The velocity-displacement or "phase-plane" diagram shown in figure 12(b) provides a convenient graphical representation of the combined motions of the container and the mass particle. In this diagram the rotating velocity-displacement vector of each container wall describes a circle of radius x_o and whose center lies on the x-axis a distance $\pm d/2$ from the origin.

Before and after impact the particle moves at a constant velocity which is represented in the phase plane by a horizontal line. Immediately before impact at point A the velocity of the particle relative to the container is $x_- - y_-$; immediately after impact it is $x_+ - y_+$. The relationship between these velocities is determined by the coefficient of restitution through the equation

$$\dot{x}_+ - \dot{y}_+ = -e\left(\dot{x}_- - \dot{y}_-\right) \tag{A2}$$

For symmetrical steady-state motion the particle velocity after impact is equal and opposite to its value before impact

$$\dot{y}_+ = -\dot{y}_- \tag{A3}$$

Also, during impact it is assumed that the driving force $F(t)$ is capable of maintaining the prescribed sinusoidal velocity of the container so that

$$\dot{x}_- = \dot{x}_+ \tag{A4}$$

From equation (A1) the container velocity at impact A ($t = 0$) is

$$\dot{x}(0) = -\omega x_o \sin \varphi \tag{A5}$$

Thus, with equations (A3) through (A5) substituted into equation (A2) the velocity of the particle immediately after impact at A is found to be

$$\dot{y}_+(0) = -\omega x_o\left(\frac{1 + e}{1 - e}\right)\sin \varphi \tag{A6}$$

Similarly the particle velocity immediately following the second impact, which occurs at B one-half an oscillation cycle later, is

$$\dot{y}_+\left(\frac{\pi}{\omega}\right) = -\omega x_o\left(\frac{1 + e}{1 - e}\right)\sin(\varphi + \pi) \tag{A7}$$

In the time interval π/ω between impacts A and B the particle travels from one end of the container to the other through a distance d. From integration of the relative velocity

$$d = \left|\int_0^{\pi/\omega} \left(\dot{y}_+ - \dot{x}(t)\right)dt\right|$$

and use of equations (A1) and (A6) this distance is

$$\frac{d}{x_o} = \left| \pi \frac{1 + e}{1 - e} \sin \varphi - 2 \cos \varphi \right| \tag{A8}$$

This equation defines the gap distance as a function of e and φ. Implicit in the equation is the assumption that upon impact the particle immediately rebounds from one side of the container and makes no further contact with the container until reaching the opposite side. When e approaches zero the particle may experience multiple impacts against the same wall or remain in contact with the wall over a significant part of the cycle. These special cases will be treated separately later in the Appendix.

Next, consider the driving force $F(t)$. With the assumption that the container mass is negligible, $F(t)$ is an impulse which exactly counteracts the impact reaction force of the mass on the container at the instant of collision. From momentum considerations the impulse is

$$\left.\begin{aligned} \lim_{\Delta t \to 0} F(0)\,\Delta t &= -2m_p \dot{y}_+(0) && \text{at A} \\ \lim_{\Delta t \to 0} F(\pi/\omega)\,\Delta t &= -2m_p \dot{y}_+(\pi/\omega) && \text{at B} \\ \text{and} \\ \lim_{\Delta t \to 0} F(t)\,\Delta t &= 0 && \text{elsewhere} \end{aligned}\right\} \tag{A9}$$

In order to derive impact damper impedance parameters c_e and m_e as expressed in the equation

$$F(t) = m_e \ddot{x} + c_e \dot{x} \tag{A10}$$

consider the following integrations over one cycle of oscillation

$$I_1 = \int_0^{2\pi/\omega} F(t)\dot{x}\, dt \tag{A11}$$

and

$$I_2 = \int_0^{2\pi/\omega} F(t)\ddot{x}\, dt \tag{A12}$$

Note that I_1 is the work per cycle done by $F(t)$ on the damper.

With the assumed form of $F(t)$ as given by equation (A10), together with time derivatives of equation (A1), these integrations produce

$$I_1 = \pi c_e \omega x_o^2 \tag{A13}$$

and

$$I_2 = \pi m_e \omega^3 x_o^2 \tag{A14}$$

From equations (A6), (A7), and (A9) the following equivalent expressions for I_1 and I_2 are obtained:

$$I_1 = 4m_p \omega x_o^2 \left(\frac{1 + e}{1 - e}\right) \sin^2\varphi \tag{A15}$$

and

$$I_2 = 4m_p \omega^3 x_o \left(\frac{1 + e}{1 - e}\right) \cos\varphi \sin\varphi \tag{A16}$$

Thus, eliminating I_1 in equations (A13) and (A15) we obtain

$$\frac{c_e}{m_p \omega} = \frac{4}{\pi}\left(\frac{1 + e}{1 - e}\right) \sin^2\varphi \tag{A17}$$

and similarly eliminating I_2 in equations (A14) and (A16)

$$\frac{m_e}{m_p} = \frac{4}{\pi}\left(\frac{1 + e}{1 - e}\right) \sin\varphi \cos\varphi \tag{A18}$$

These expressions for the equivalent viscous damping and effective mass, together with equations (A8), which relates d/x_o to φ, define the impact damper impedance for the previously stated assumptions regarding rebound conditions. In relating these equations to the chain damper, the mass m_p is replaced by the total chain mass lm under the assumption that impact occurs along the full length of the chain. Equations (A17) and (A18) with e as a parameter are plotted as a function of d/x_o in figure 5.

As mentioned earlier when $e \to 0$ the particle does not rebound after impact. For the condition $e = 0$, rather than following the rectangular path shown in figure 12(b), the particle remains in contact with the container after impact at A until the container accelerates to its maximum velocity. It then separates from the container with an absolute velocity of $-\omega x_o$ which is retained until impact at B on the opposite side. The process is then repeated.

To account for conditions of zero elastic rebound ($e = 0$), it is necessary to modify the preceding analysis as follows: The force term $F(t)$ will include, in addition to the impulse due to impact, an inertia force $m_p\ddot{x}$. This additional force acts from the time of impact until the particle separates from the container wall at the time $\ddot{x}$ changes sign. Also, the velocity of the particle prior to impact $\left(\text{i.e., } |\dot{y}_-| = \omega x_o\right)$ differs from that derived from equation (A2). With these modifications applied to the foregoing analysis, the impedance equations for $e = 0$ are found to be

$$\left.\begin{aligned} \frac{c_e}{m_p\omega} &= \frac{1}{\pi}\left(1 + \sin\varphi\right)^2 \\ \frac{m_e}{m_p} &= \frac{1}{2} - \frac{1}{\pi}\varphi + \frac{2}{\pi}\cos\varphi + \frac{1}{2\pi}\sin 2\varphi \end{aligned}\right\} \qquad \text{(A19)}$$

where

$$\frac{d}{x_o} = \left|\frac{\pi}{2} + \varphi - \cos\varphi\right|$$

It should be noted that these equations are applicable for $-\pi/2 \leqq \varphi \leqq \pi/2$; for φ values beyond this range the container accelerates away from the particle immediately after impact, therefore, the previously developed impedance equations are appropriate. In figure 5 the curves for $e = 0$ were determined from both sets of equations with the transition from one set to the other occurring at $\varphi = \frac{\pi}{2}$ $(d/x_o = \pi)$.

Stability Boundaries

The region of steady two-impact-per-cycle motion as a function of d/x_o and e is shown in figure 7. The boundary on the right represents the maximum allowable value of d/x_o and the boundary on the left, the minimum allowable value. To determine the upper limit on d/x_o we maximize equations (A8) with respect to φ

$$\frac{\partial\left(\frac{d}{x_o}\right)}{\partial\varphi} = \pi\left(\frac{1 + e}{1 - e}\right)\cos\varphi + 2\sin\varphi = 0$$

from which the critical value of φ is

$$\varphi_{crit} = \tan^{-1}\frac{-\pi(1 + e)}{2(1 - e)}$$

where for $0 \leqq e \leqq 1$, $122.5^\circ \leqq \varphi_{crit} \leqq 90^\circ$. Thus, the upper limit on d/x_o becomes

$$\left(\frac{d}{x_o}\right)_{crit} = \left|\pi\left(\frac{1 + e}{1 - e}\right)\sin\varphi_{crit} - 2\cos\varphi_{crit}\right| \qquad \text{(A20)}$$

The minimum allowable d/x_o for two-impact-per-cycle motion may be found as follows: With reference to figure 12(b) let ϵ be the separation distance between the particle and the container immediately following an impact at point A. If this distance becomes zero as the container accelerates to maximum velocity, a second impact will occur. It can be seen that the container reaches

maximum velocity at the time $\frac{\pi/2 - \varphi}{\omega}$ seconds after impact at A. Thus, the separation distance at this time is

$$\epsilon = \left| \int_0^{\frac{\pi/2 - \varphi}{\omega}} \left(\dot{y}_+ - \dot{x}_+ \right) dt \right|$$

From equations (A5) and (A6)

$$\epsilon = x_o \left| \frac{(1 + e)(\pi/2 - \varphi)\sin \varphi}{1 - e} - \cos \varphi \right| \tag{A21}$$

Therefore, $\epsilon = 0$ when

$$(1 + e)(\pi/2 - \varphi) = (1 - e)\frac{\cos \varphi}{\sin \varphi}$$

or

$$e = \frac{\cot \varphi - \frac{\pi}{2} + \varphi}{\cot \varphi + \frac{\pi}{2} - \varphi} \tag{A22}$$

This equation in combination with equation (A8) for d/x_o then defines the left boundary plotted in figure 7.

REFERENCES

Arnold, R. N.: Response of an Impact Vibration Absorber to Forced Vibration. 9th Congrès International Mécanique Appliquée, University of Brussels, vol. 7, 1957, pp. 395-418.

Egle, D. M.: An Investigation of an Impact Vibration Absorber. Presented at the ASME Vibrations Conference, Boston, Mass., March 29-31, 1967, ASME Paper No. 67, Vibr-10. To be published in the Jour. Engr. for Industry.

Farmer, Moses G.; and Reed, Wilmer H. III: Study of Wind Excited Oscillations of High Band Wullenwebber Antenna. NASA LWP-324, November 1966.

Foughner, Jerome T., Jr.; and Duncan, Rodney L.: A Full-Scale Ground Wind Load Research Program. Compilation of Papers Presented at the NASA Langley Research Center at the Meeting on Ground Wind Load Problems in Relation to Launch Vehicles, June 7-8, 1966, NASA TM X-57779.

Lieber, P.; and Jensen, D. P.: An Acceleration Damper: Development, Design, and Some Applications. Trans. ASME, vol. 67, 1945, pp. 523-530.

Masri, Sami F.: Electric-analog Studies of Impact Dampers. Experimental Mechanics, vol. 7, no. 2, February 1967, p. 49.

Reed, Wilmer H. III; and Duncan, Rodney L.: Dampers to Suppress Wind-Induced Oscillations of Tall Flexible Structures. Presented at the 10th Midwestern Mechanics Conference, Fort Collins, Colorado, August 21-23, 1967.

Warburton, G. B., discussion of Grubin, C.: On the Theory of the Acceleration Damper. Journal of Applied Mechanics, vol. 24, Trans. ASME, vol. 79, 1957, pp. 322-324.

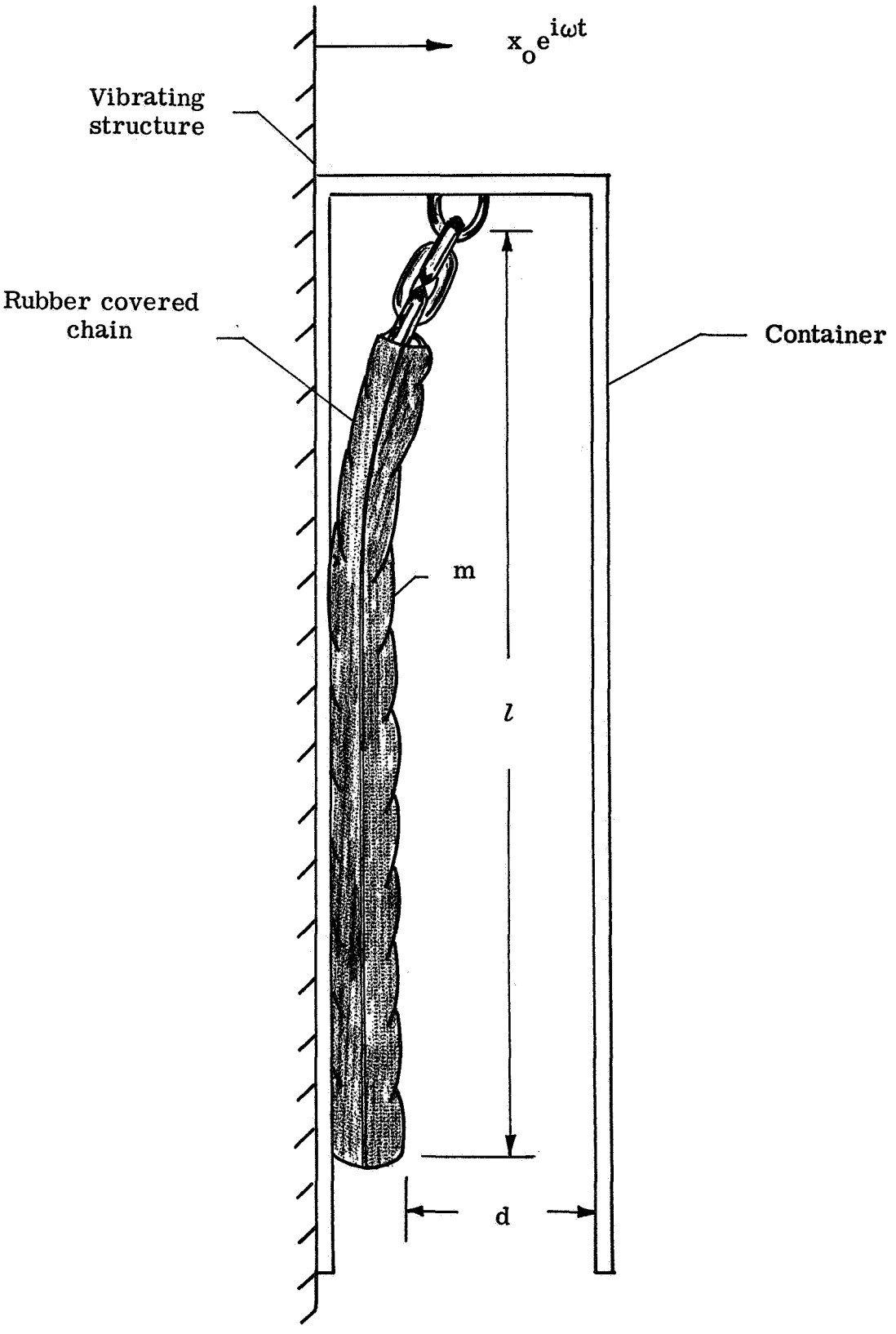

Figure 1.- Chain damper configuration studied.

Chain damper on vibrating structure

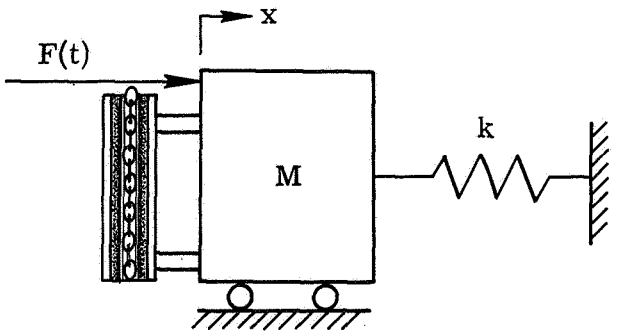

$$F(t) = \underbrace{\left[M\ddot{x} + kx\right]}_{\text{Structure}} + \underbrace{\left[m_e\ddot{x} + c_e\dot{x}\right]}_{\text{Damper}}$$

Mechanical impedance representation

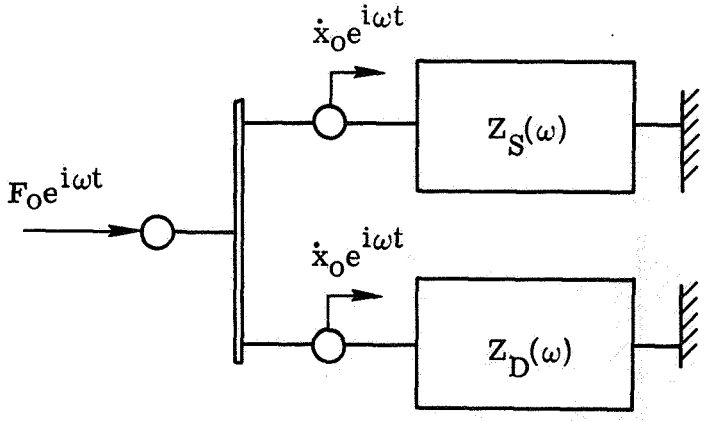

$$F_o = \left[Z_S(\omega) + Z_D(\omega)\right]\dot{x}_o$$

Figure 2.- Mechanical impedance representation of chain damper attached to a vibrating structure.

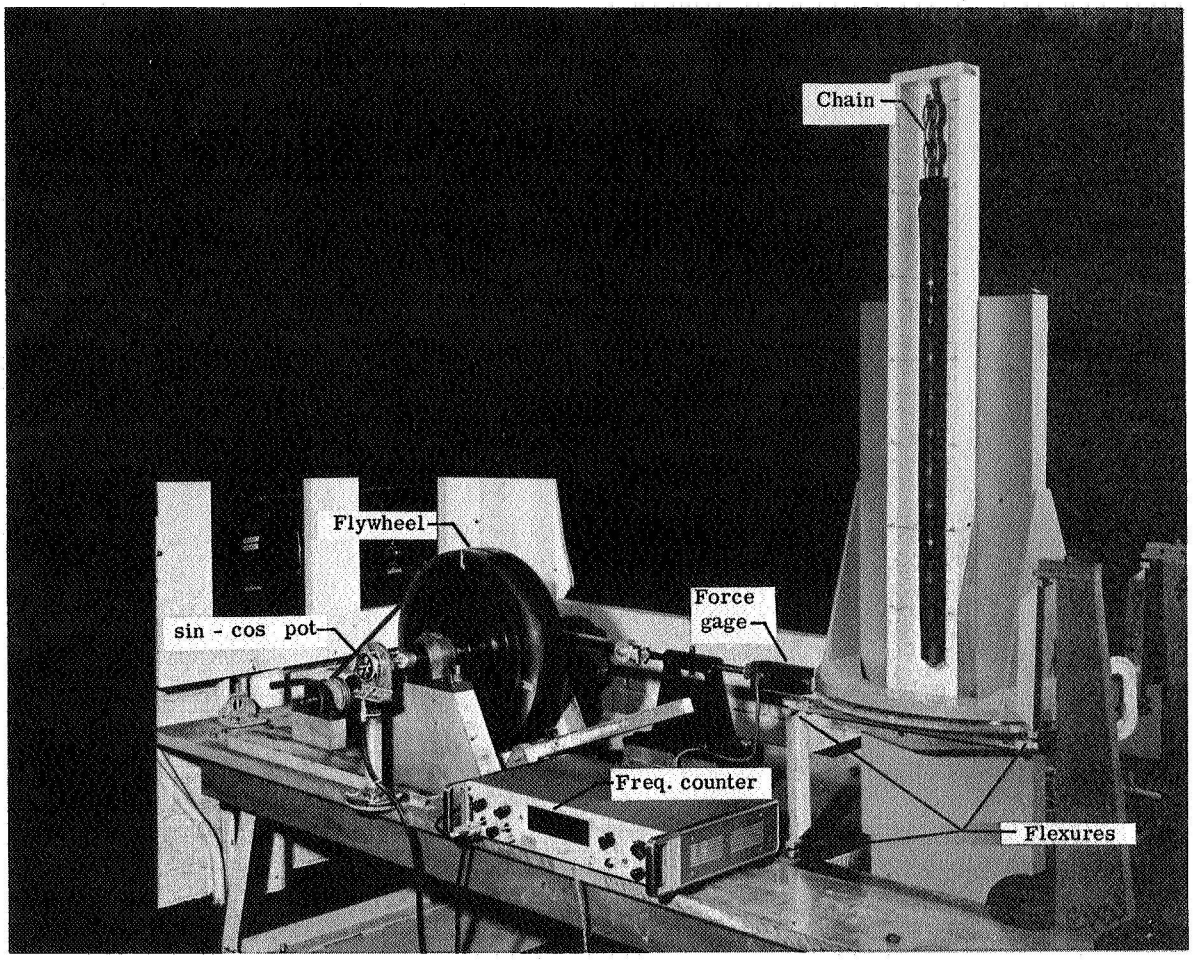

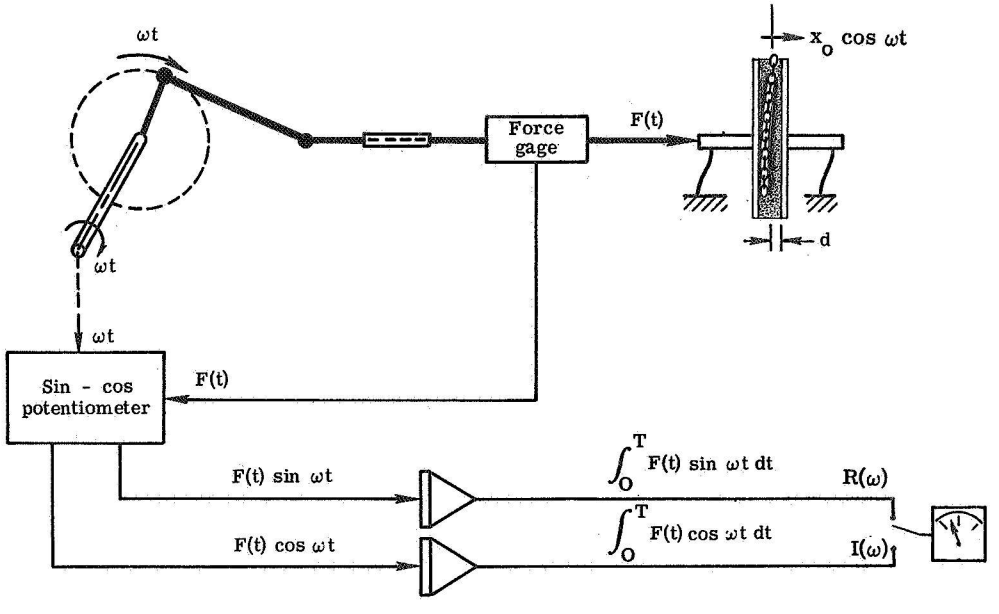

Figure 3.- Mechanical impedance test apparatus and data-reduction procedure.

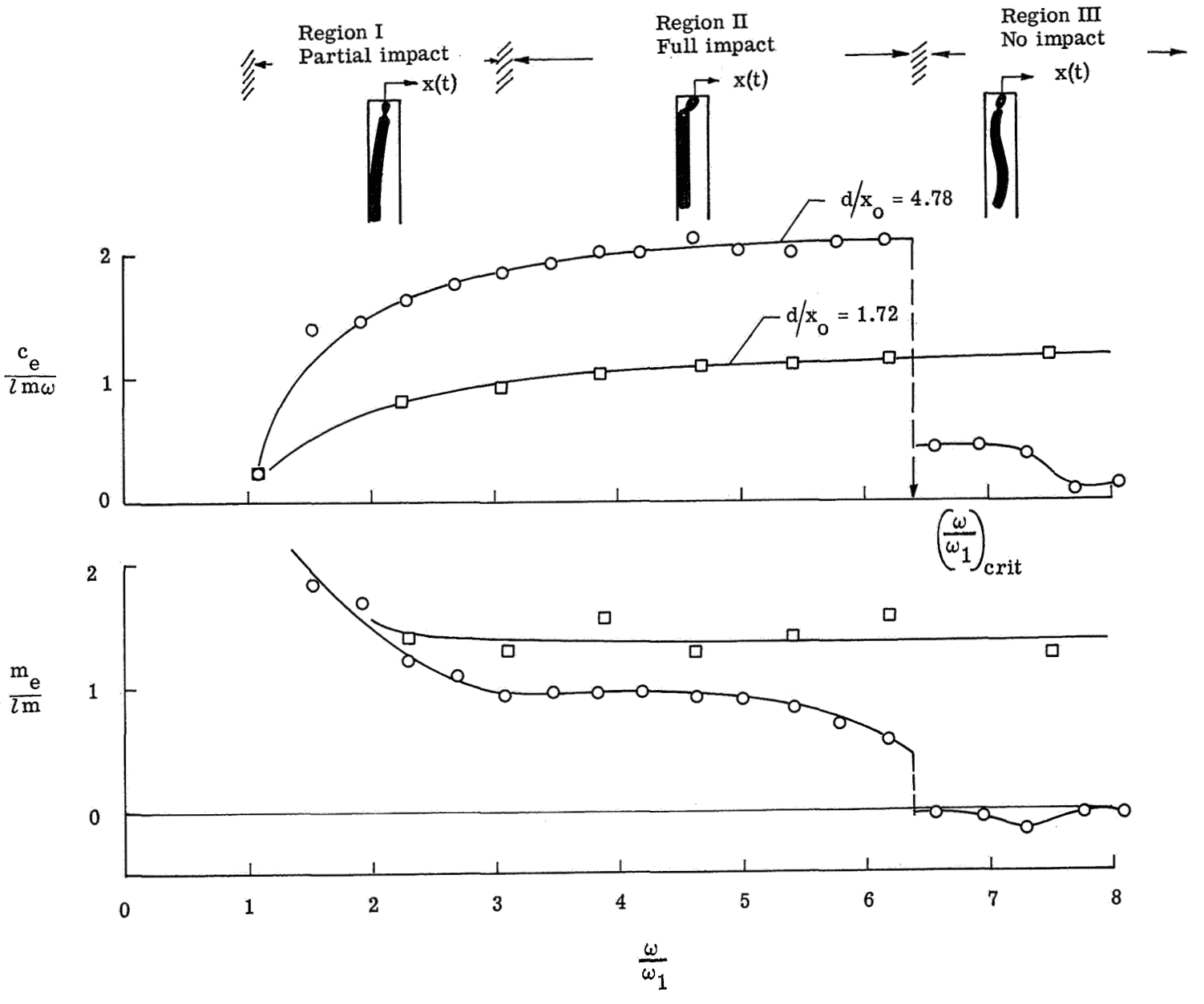

Figure 4.- Effect of frequency ratio on damper impedance.

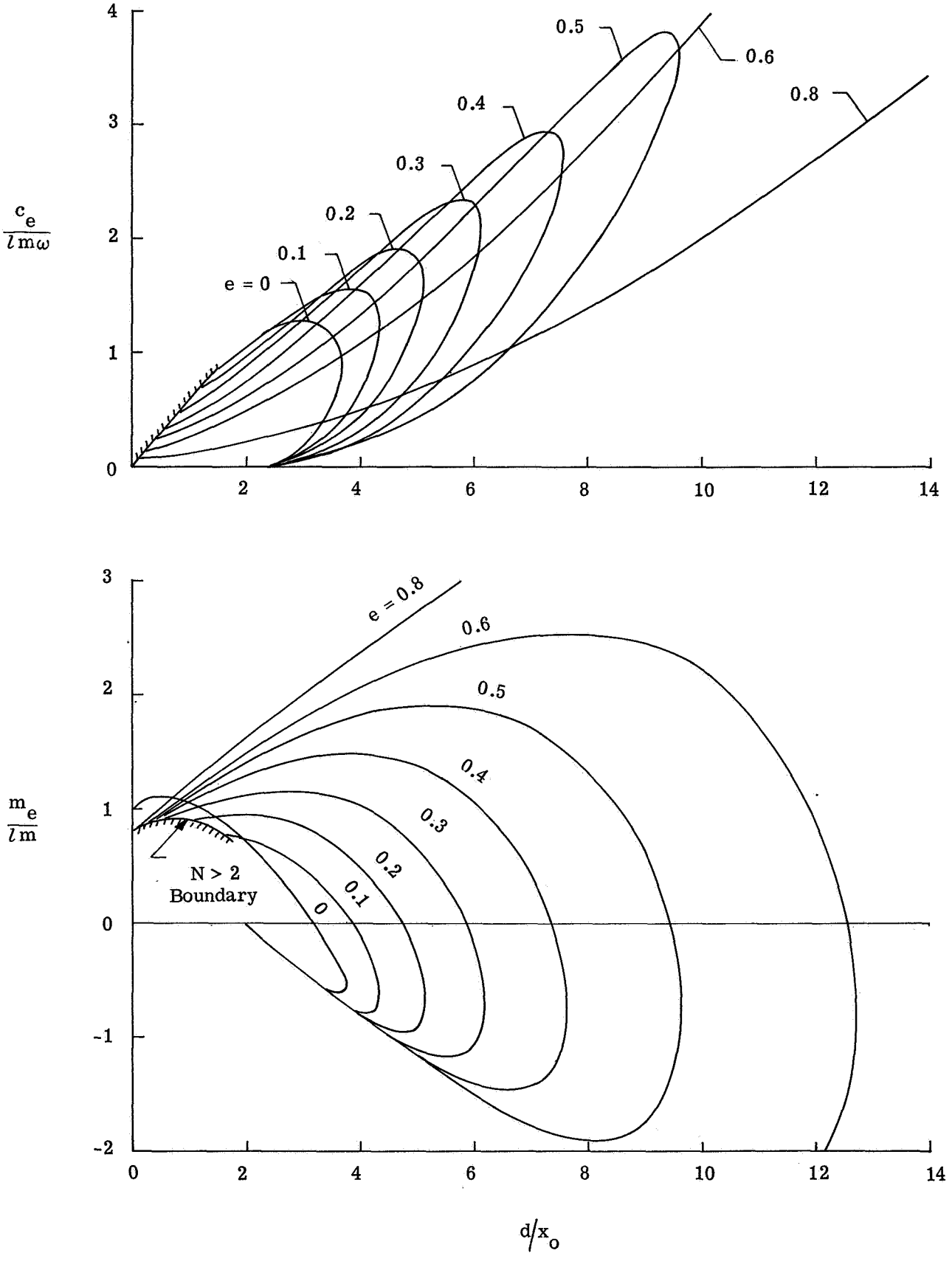

Figure 5.- Theoretical impact damper impedance functions.

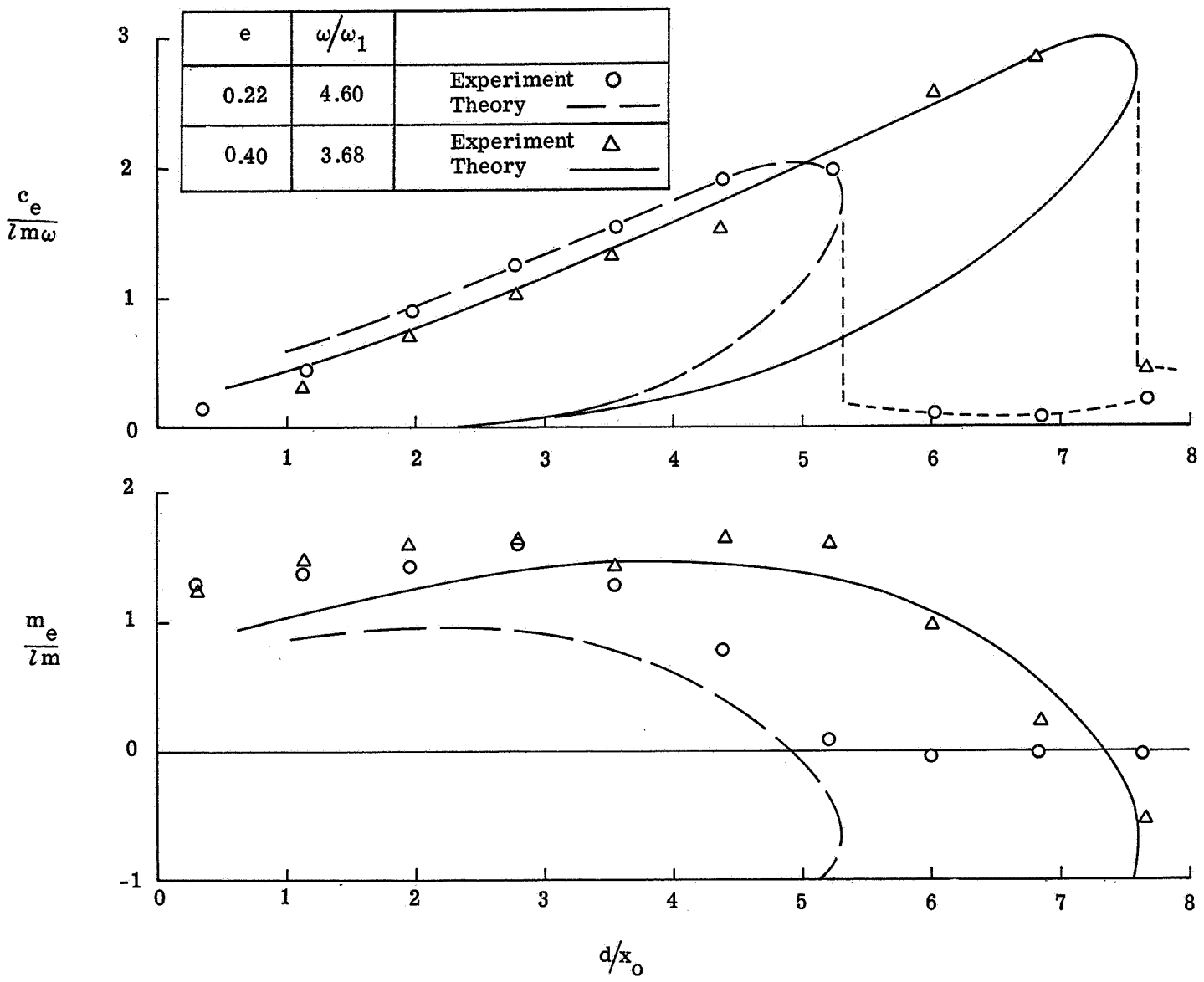

Figure 6.- Effect of gap ratio on measured and predicted damper impedance.

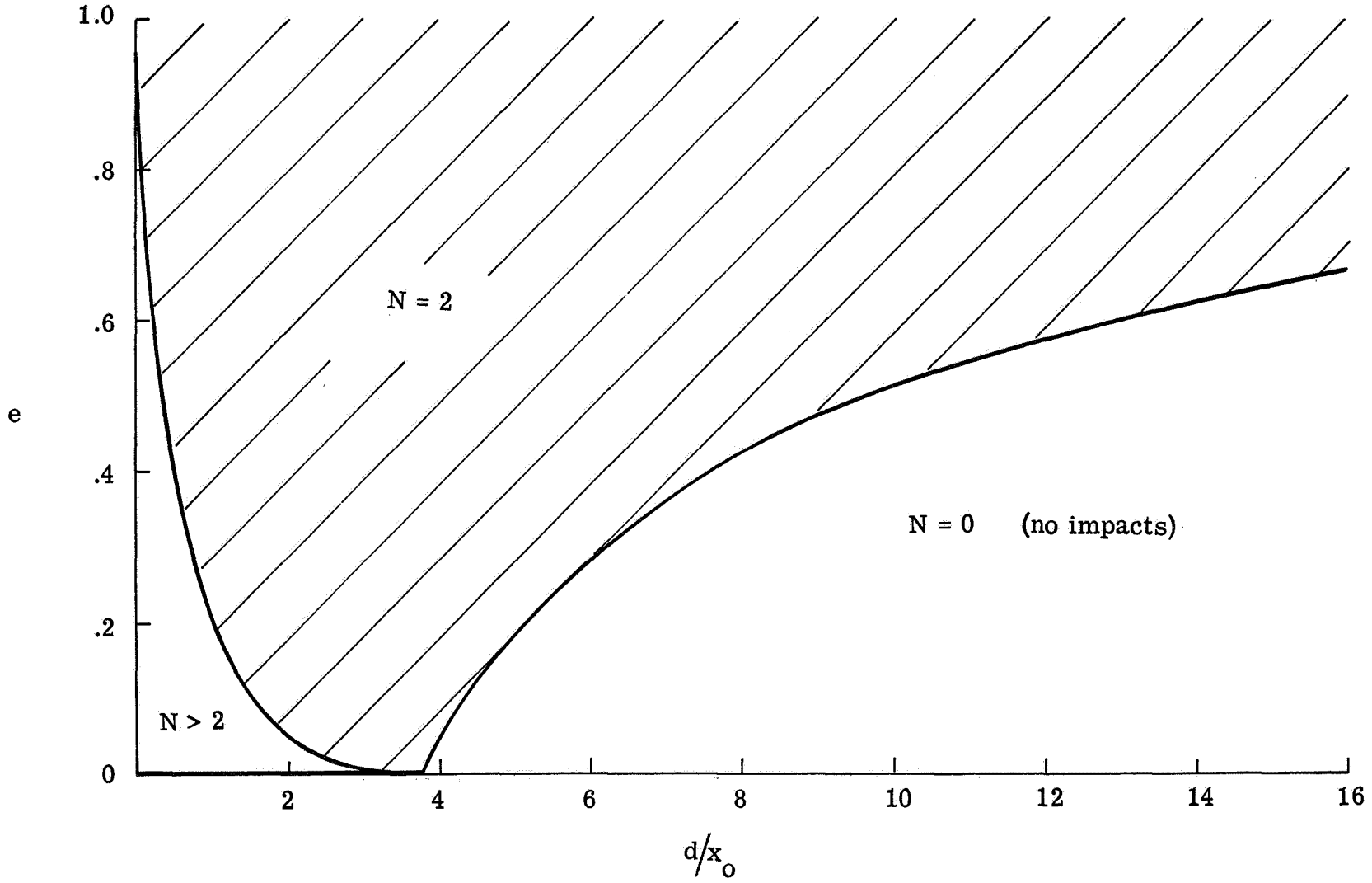

Figure 7.- Boundaries for two-impact-per-cycle motion of damper mass.

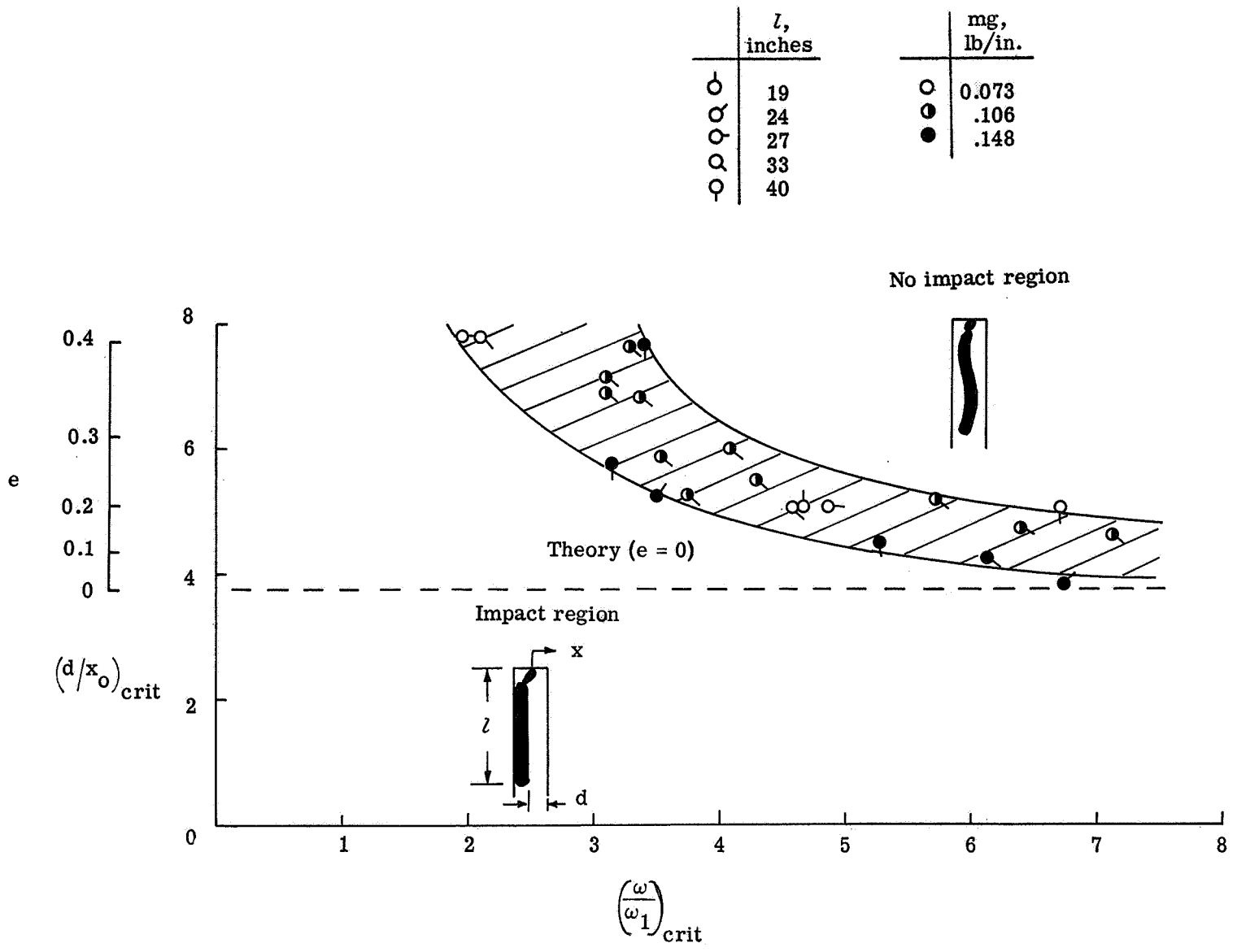

Figure 8.- Impact stability boundary measurements on chain dampers.

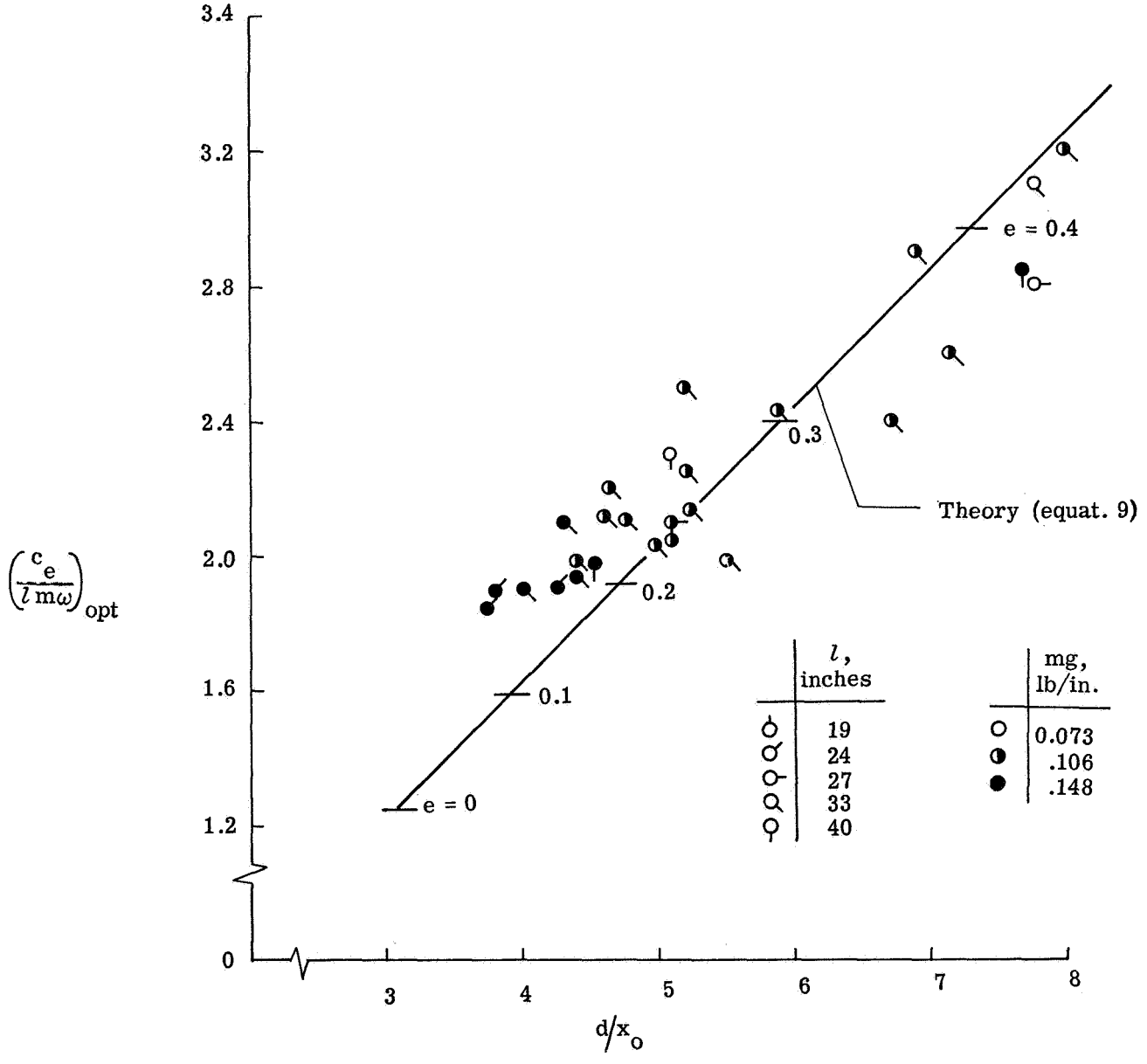

Figure 9.- Optimum damping as gap distance.

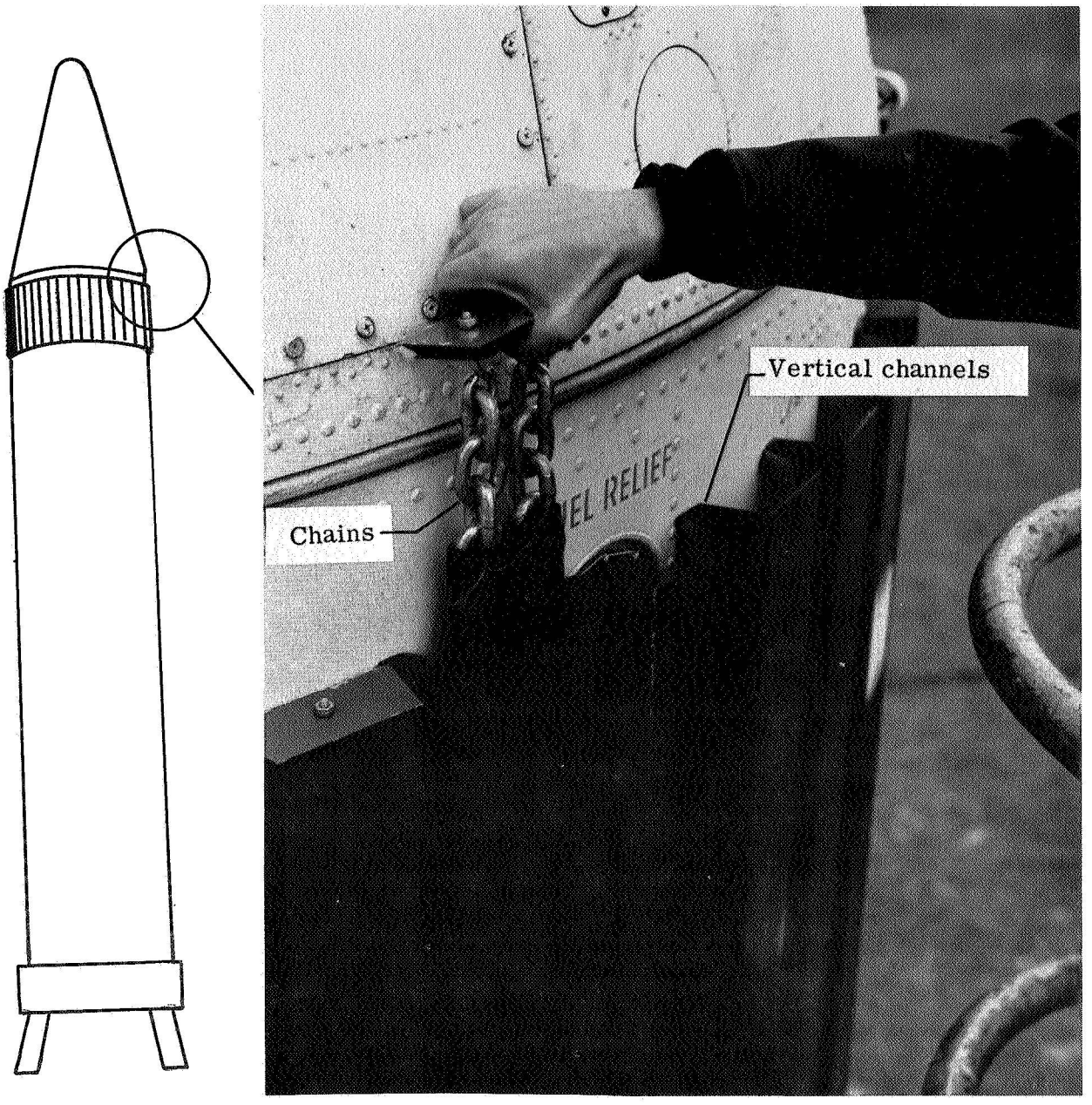

Figure 10.- Chain damper installation on Jupiter launch vehicle.

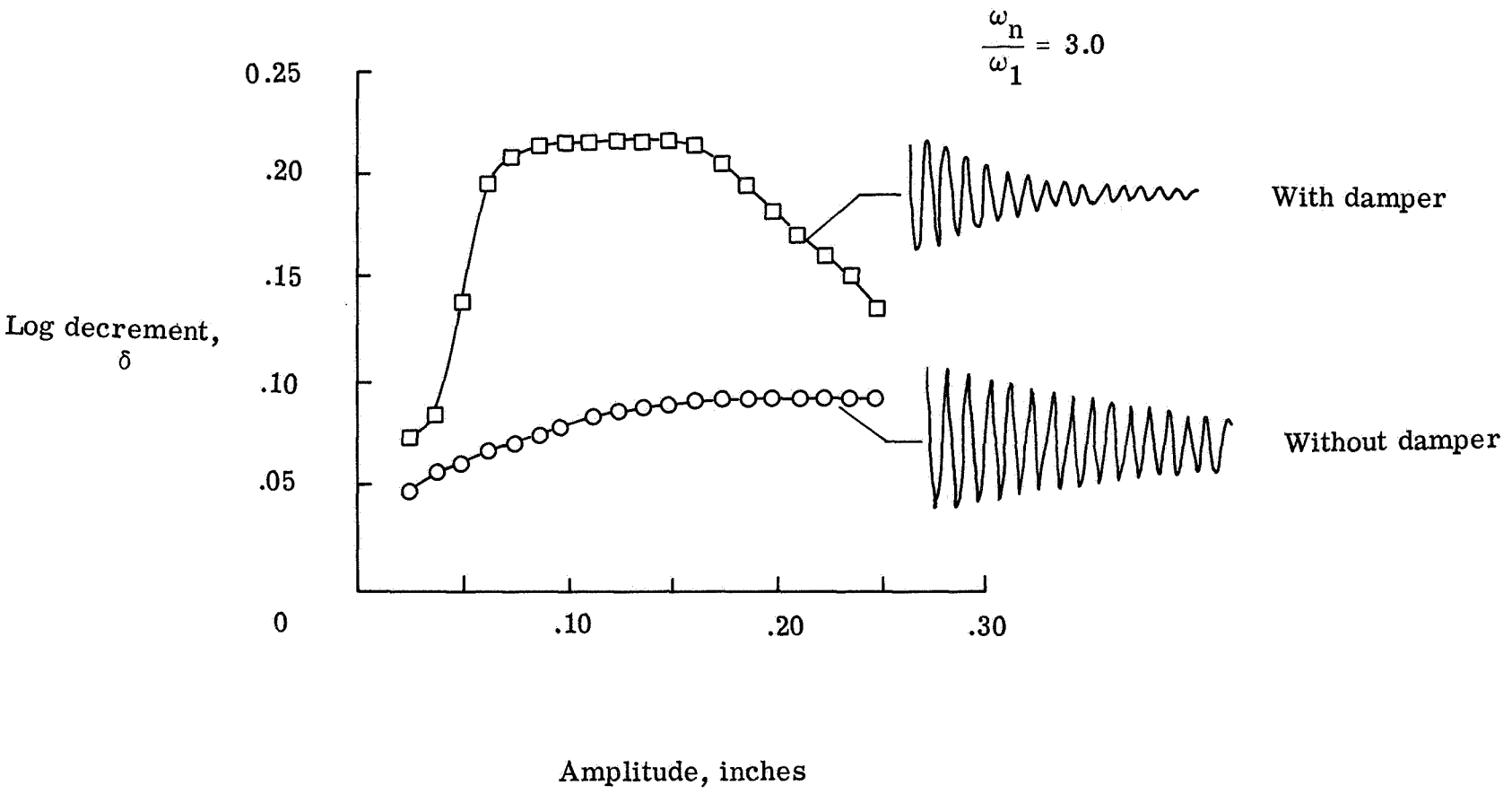

Figure 11.- Effect of chain dampers on Jupiter vehicle damping.

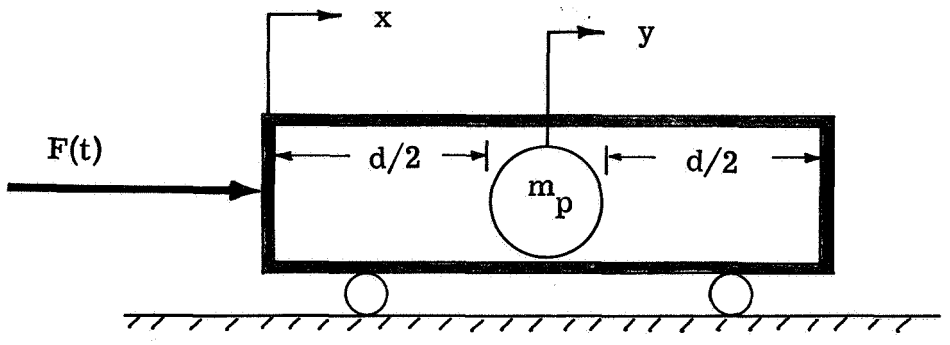

(a) Model of system.

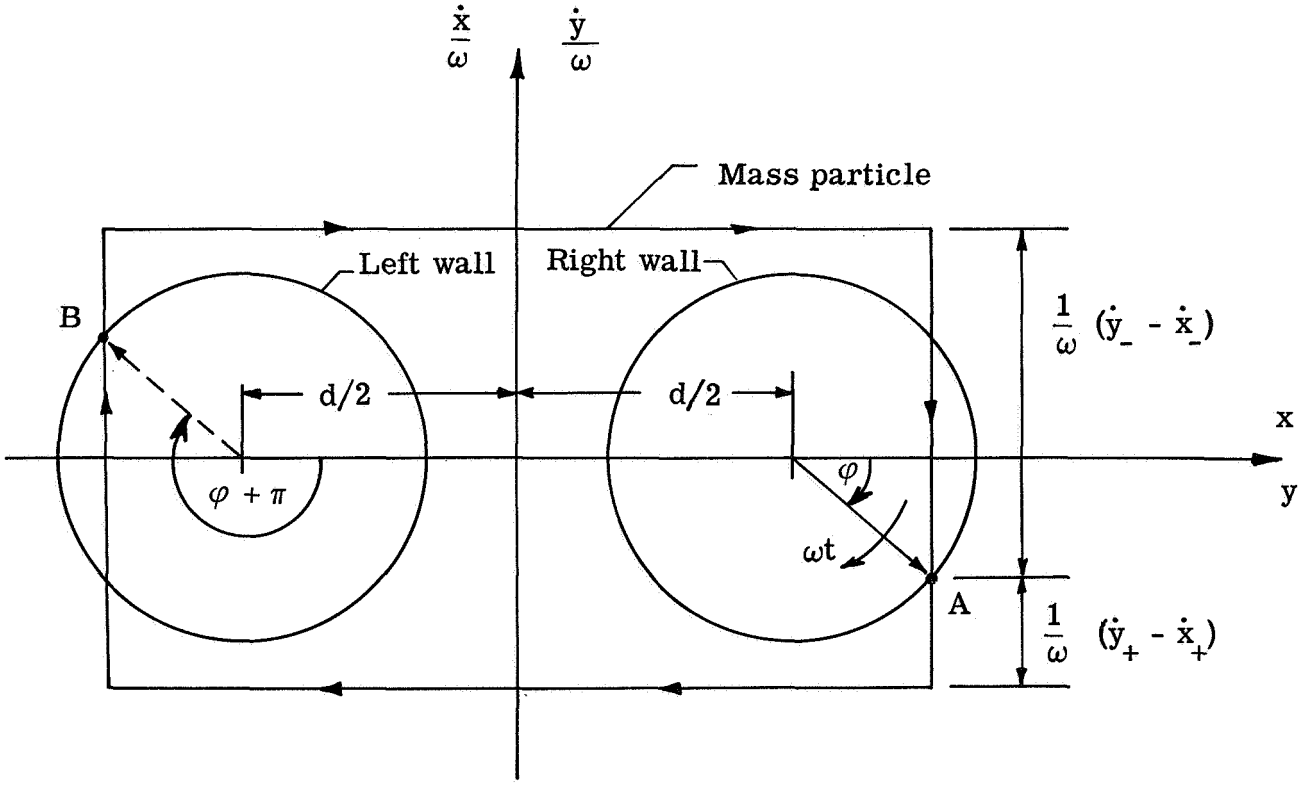

(b) Phase plane representation of particle and container motions for $e > 0$.

Figure 12.- Idealized single-particle impact damper.

NASA-Langley, 1967